Report No. 54EFS31 Nov. 1954

DEVELOPMENT OF A CONSTANT-FORCE BOTTOM CONTOUR FOR SEAPLANE HULLS

By
E. F. Schulz

Department of Civil Engineering

Colorado Agricultural and Mechanical College
Fort Collins, Colorado

DEVELOPMENT OF A CONSTANT-FORCE BOTTOM CONTOUR FOR SEAPLANE HULLS

by

E. F. Schulz
Civil Engineering Department
Colorado A & M College
Fort Collins, Colorado

prepared for
Bureau of Aeronautics
Navy Department
under Contract No. NOas52-332-c
through the
Colorado A & M Research Foundation

TABLE OF CONTENTS

Chapter

LIST OF TABLES

LIST OF FIGURES

NOTATIONS AND DEFINITIONS

Symbol	Units	Definition
M	slugs	Mass of wedge or hull
z	in.	Displacement of keel below pile-up
z'	in.	Displacement of keel below static water surface
$\dot{z}$, v	in/sec	Velocity of hull
v_o	in/sec	Initial velocity of hull at contact with water surface
m	slugs	Apparent mass of water
ρ	slugs/cu ft	Mass density of water
β	degrees	Angle of deadrise
β_e	degrees	Equivalent angle of deadrise
t	sec	Time
μ	--	Ratio of masses, m/M
c	in.	Half wetted width of hull with piled-up water
c'	in.	Half wetted width of hull assuming no piled-up water
x	in.	Horizontal coordinate of any point
g	in/sec^2	Acceleration of gravity
f_u	lb	Unsteady-state force
f_s	lb	Steady-state force
f_b	lb	Buoyant force
Γ	--	Gamma function

Symbol	Units	Definition
η	in.	Ordinate to free water surface measured from keel
a	in/sec^2	Effective acceleration of gravity in g's = 1 - L/W
n	--	Load factor f/W
r	--	Efficiency factor of force-displacement curve

FOREWORD

This report represents an extension of the theoretical and experimental work carried out at Massachusetts Institute of Technology by Prof. R. L. Bisplinghoff and Mr. C. S. Doherty. This experimental work was sponsored at Colorado A & M College by the Bureau of Aeronautics, Department of the Navy.

The author is indebted to Mr. H. I. Flomenhoft and Mr. F. W. S. Locke, Jr. of the Bureau of Aeronautics for much encouragement and assistance in the conduct of the work and the preparation of this report. The author wishes to thank Dr. D. F. Peterson Head of Department of Civil Engineering and Dr. M. L. Albertson, Head of Fluid Mechanics Research at Colorado A & M College for advice in the conduct of the research work and for assistance in the preparation of the report. Assistant Professor C. C. Britton of the Electrical Engineering Department and Assistant Professor H. H. Schweizer of the Civil Engineering Department were consulted in connection with the instrumentation problems. Prof. T. H. Evans is Dean of Engineering.

Chapter I

INTRODUCTION

Any possibility of reducing the structural weight of a modern airplane is worthy of careful consideration. The size and strength of many structural components of modern aircraft are dictated by the loads occurring during landing, particularly for the seaplane landing in rough-water conditions. In the case of the seaplane, it is theoretically possible to derive a bottom contour which will yield the smallest maximum (peak) deceleration to absorb a given kinetic energy at contact. Experimental verification of a theoretically derived constant-force hull shape has been disappointing. Results indicated that more should be learned about the water-entry phenomenon of hulls having small angles of deadrise. The purpose of this report is to describe further the details of experiments on the water pile-up and the deceleration history of the constant-force hull shape as an approach to the development of the optimum hull contour.

Other Applications of the Water Entry Problem

The condition of entry of solid bodies into a mass of water has been brought into sharp focus in recent years. The designers of naval ordnance, ship hulls, and seaplanes have been concerned with various phases of water entry. The theory is based on assumptions regarding the apparent mass of water which is considered to be affected by the impact of the body. The theoretical approach is complicated by the pile-up of water immediately adjacent to the hull.

The Techniques Employed in This Investigation

In this investigation the pile-up phenomenon was measured from still photographs taken at a high speed. The acceleration histories of the hulls were obtained by photographing the output of an electronic accelerometer mounted in the hull from an oscilloscope screen. During these experiments the test hulls were permitted to fall freely into the test tank.

The pile-up was measured on 8- x 10-in. enlargements of the still photographs. Measurements confirmed previous findings in that the theoretical approach to the problem failed to describe the water pile-up satisfactorily. These experiments also verified the difficulty in obtaining good photographs of the water pile-up for the $\beta = 10^{\circ}$ hulls.

This is due primarily to the fact that the whole impact phenomenon occurs in a time period of less than 0.05 sec.

A bottom contour developing a constant acceleration history has been developed by a trial and error process. The starting point was the shape developed from the theoretical approach. The experimentally-developed hull shape retains the low values of deadrise over a greater part of the total beam width than the theoretical hull shape. The majority of the work was conducted on a hull whose equivalent angle of deadrise was 20°. Hulls of equivalent angles of deadrise of 30° and 40° were also tested. The equivalent angle of deadrise is defined as the angle made with the horizontal by a straight line joining the keel and the chine.

Chapter II

REVIEW OF LITERATURE

Early Investigation

Early theory was developed for a V-wedge by von Kármán (1) in 1929 based on the assumption that the momentum of the hull is transferred to the momentum of an apparent mass of water. For the case of two-dimensional flow, the apparent mass was assumed to be a half cylinder of water of diameter equal to the submerged width 2c of the wedge and length L equal to the length of the hull. This situation can be described as an example of conservation of momentum between the hull and apparent mass of water. The mathematical expression of this condition is:

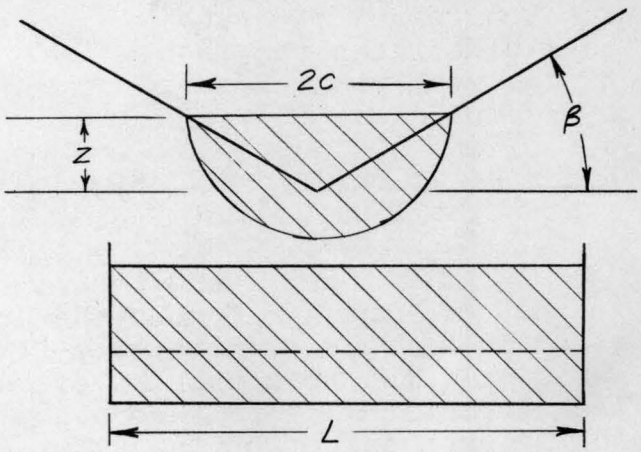

Fig. 2.1 Diagram of assumed apparent mass for two-dimensional hull

$$M\, v_o = (M + m)\, v \qquad (2.1)$$

Von Kármán showed the solution of Eq. 2.1 to be:

$$dv/dt = - \frac{2\, v_o^2}{z(1 + \mu)^3}$$

where $\mu = m/M$

and $t = \frac{z}{v_o} (1 + \mu/3)$

Von Kármán's work did not account for the pile-up of water above the static surface adjacent to the hull. Wagner in 1932 first considered the pile-up of water adjacent to

the hull. Later Monaghan added to Wagner's work giving a formula relating the apparent mass of the water with the wetted width associated with the static water surface,

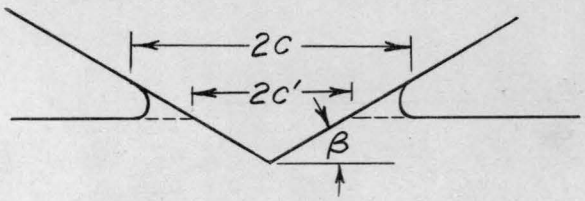

Fig. 2.2 Definition sketch for water pile-up on a V-wedge hull

$$c = \pi/2\,(1 - \beta/\pi)\,c' . \qquad (2.2)$$

Bisplinghoff and Doherty(5) show a similar development to that of Monaghan by considering the hull to be an expanding prism in a field of potential flow. The flow around the prism was simplified to a problem of rectilinear flow by a conformal transformation. This theoretical analysis resulted in the following expression for the water pile-up (5:32):

$$c/c' = \frac{\pi \tan\beta}{2K\beta} , \qquad (2.3)$$

where K is the scale factor for the transformation and is

$$K = \frac{\sqrt{\pi}}{\Gamma(1/2 + \beta/\pi)\,\Gamma(1 - \beta/\pi)\cos\beta} . \qquad (2.4)$$

Therefore, Eq. 2.3 becomes:

$$c/c' = \sqrt{\pi}/2\,\frac{\sin\beta}{\beta}\,\Gamma(1/2 + \beta/\pi)\,\Gamma(1 - \beta/\pi). \qquad (2.5)$$

Fig. 5.1 shows the solution of Eq. 2.5.

Further refinements were made in the theoretical analysis by other writers by accounting for such factors as the steady-state force and partial wing lift.

Recent Investigations

Most previous work has been summarized by Bisplinghoff and Doherty (5) in 1950. They extended the theory of the previous investigations and conducted a systematic study of the significance of various factors. The hull was considered to be a two-dimensional V-wedge entering the water with the for on the hull composed of three parts:

1. The unsteady-state force f_u caused by change of the momentum of the apparent mass,

2. Skin friction drag f_s or the steady-state force,

3. Force of buoyancy f_b .

Because of uncertain accuracy of the theoretical values of the steady-state drag coefficient, experimental values were obtained for 10°, 20°, 30°, and 40° wedge models by conducting tests in a water tunnel.

An experimental check of calculated impact loads was obtained by dropping larger V-wedge models vertically into a tank. The acceleration-time history was determined by recording the output from a Statham accelerometer with an oscillograph. The pile-up of the water was recorded by photographing the impact phenomenon through a glass panel in the front of the tank, using a 16 mm high-speed motion picture camera operating at 1500 fromes per second. The following conclusions were reached from the investigations of reference (5):

1. Experimental data showed no correlation with theory regarding the pile-up of water and consequently with apparent mass.

2. Experimentally determined peak decelerations were much less than theoretical values at $\beta = 10°$, agreeing in the 20 tc 30° range, and becoming higher than theoretical values at the higher values of deadrise.

3. The buoyancy force f_b was negligible.

4. The steady-state force f_s was larger than f_b , but smaller when compared to f_u .

5. The unsteady-state force f_u was clearly the predominant factor (5:67).

A comparison of the results of each of five theories was made with the experimental results for the $\beta = 20^{\circ}$ hull. The comparison indicated generally similar results for all the theoretical equations. The method of Kreps indicated considerably greater values than the experimental results and the method of von Kármán being somewhat less than the experimental values.

The apparent mass of water computed from the peak values of the acceleration history curves for each theoretical method was compared with the experimental values. The trends established for the experimental points bore no resemblance to the theoretical curves. The acceleration histories determined from each of the five theoretical methods and the experimental results were also compared by consideration of the maximum acceleration and the time to maximum acceleration.

Bisplinghoff and Doherty developed a theoretical constant-force bottom contour. An experimental model of the constant-force hull bottom was constructed and tested, but the agreement between the theoretical acceleration history and the experimental history was poor. The experimental hull failed to develop a sufficient value of deceleration during the early period when the angle of deadrise was small. The authors concluded that the failure of the theory was due to a questionable assumption of an incompressible fluid and to the lack of understanding of the nature of water pile-up at low deadrise angles.

Summary

The investigations of seaplane impact to date indicate that there is a lack of understanding of the mechanics of water entry, particularly for low angles of deadrise.

Chapter III

THEORETICAL ANALYSIS

The theoretical analysis logically falls into two general considerations:

1. Development of the bottom contour to experience any assumed force-time history.
2. Development of the bottom contour to produce a constant force during impact.

Development of the Bottom Contour for any Force-time History

If the acceleration of the hull at any time can be considered to be a function of the displacement, then

$$a = \phi(z)$$

and

$$dv/dt = \phi(z) ,$$

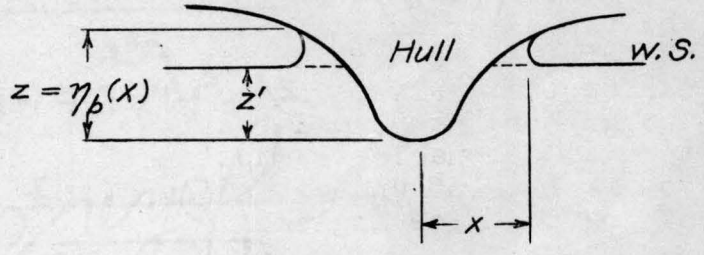

Fig. 3.1 Definition sketch for water pile-up on any hull

furthermore

$$\frac{dv}{dt} = \frac{dv}{dz}\frac{dz}{dt} = \phi(z) ,$$

or

$$v\, dv = \phi(z)dz . \qquad (3.1)$$

Integrating Eq. 3.1 ,

$$\frac{v^2}{2} = \int_o^{z_f} \phi(z)\, dz + \frac{v_o^2}{2} . \qquad (3.2)$$

However, from Eq. 2.1 , assuming full wing lift,

$$v = v_o/(1 + \mu) , \qquad (3.3)$$

where

$$\mu = m/M \ .$$

Substituting Eq. 3.3 in Eq. 3.2:

$$\frac{v_o^2}{2(1+\mu)^2} = \int_o^{z_f} \phi(z)\, dz + v_o^2/2 \qquad (3.4)$$

Solving for μ :

$$\frac{1}{(1+\mu)^2} = \frac{2}{v_o^2}\int_o^{z_f} \phi(z)\, dz + 1 \qquad (3.5)$$

$$(1+\mu)^2 = \frac{1}{2/v_o^2 \int_o^{z_f} \phi(z)\, dz + 1}$$

$$\mu = \frac{1}{\sqrt{2/v_o^2 \int_o^{z_f} \phi(z)\, dz + 1}} - 1 \qquad (3.6)$$

But $1/2\ M\ v_o^2$ represents the energy at impact to be absorbed by the water. The energy absorbed is equal to the area under the force-displacement curve (solid line) as shown in Fig. 3.2.

If r is a shape efficiency factor relating the area of the given curve to the area of the dotted rectangle, then

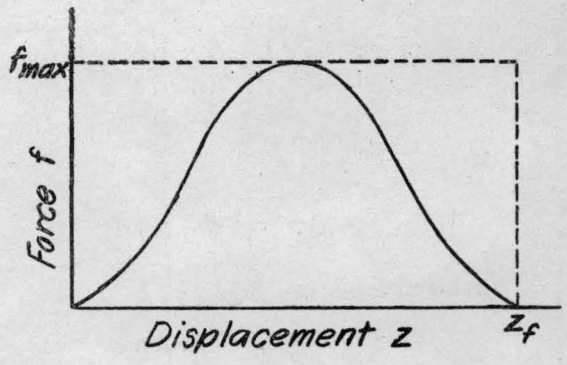

Fig. 3.2 Force-displacement diagram

$$1/2\ M\ v_o^2 = (f_{max}\ z_f)\ r \qquad (3.7)$$

where z_f is the displacement when v becomes zero. If $f_{max} = n_{max}W$ where n is a load factor, then Eq. 3.7 becomes

$$\tfrac{1}{2}(W/g)\ v_o^2 = r\ n_{max} z_f\ W$$

or

$$n_{max} = \frac{v_o^2}{2gr\ z_f}\ , \tag{3.8}$$

rearranging

$$\frac{2}{v_o^2} = \frac{1}{n_{max} gr\ z_f}\ . \tag{3.9}$$

Substituting Eq. 3.9 in Eq. 3.6

$$\mu = \frac{1}{\sqrt{\frac{1}{n_{max} gr\ z_f}\int_o^{z_f} \phi(z)dz + 1}} - 1 \tag{3.10}$$

If $f_{max} = n_{max}\ W$ then,

$$f(z) = n(z)W\ , \text{ and}$$

$$f(z) = Wa/g$$

then,

$$\phi(z) = n(z)g\ . \tag{3.11}$$

Substituting Eq. 3.11 in 3.10 and simplifying:

$$\mu = \frac{1}{\sqrt{\frac{1}{r}\int \frac{n(z)}{n_{max}}\ d\ \frac{z}{z_f} + 1}} - 1\ . \tag{3.12}$$

By definition,

$$\mu = \frac{m}{M} = D^2 \frac{\pi \rho x^2}{2M} , \qquad (3.13)$$

where D is a constant which accounts for the effect of deadrise and pile-up on the apparent mass.

The Constant-force Bottom Contour

If a hull is assumed to have the constant-force bottom contour, then its force-displacement diagram would describe the dotted rectangle in Fig. 3.2. If Eq. 3.11 is correct then Fig. 3.2 would be equivalent to Fig. 3.3; then $n(z) = -n_{max}$ and $r = 1$.

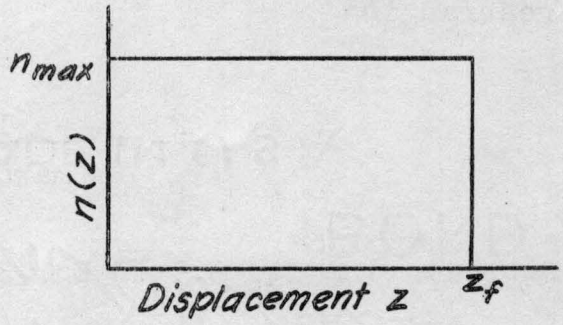

Fig. 3.3 Acceleration-displacement diagram for ideal case

For this condition of an actual constant-force hull, Eq. 3.12 becomes:

$$\mu = \frac{1}{\sqrt{-\int d \frac{z}{z_f} + 1}} - 1 .$$

Integrating

$$\mu = \frac{1}{\sqrt{1 - z/z_f}} - 1 . \qquad (3.14)$$

Equating Eq. 3.13 and 3.14

$$D \sqrt{\frac{\pi \rho}{2M}}\, x = \sqrt{\frac{1}{\sqrt{1 - z/z_f}} - 1} \qquad (3.15)$$

The condition indicated by Eq. 3.15 is evaluated in the following table:

Table 3.1

Dimensionless Coordinates of Theoretical Constant-force Bottom Contour

z/z_f	$D\sqrt{\frac{\rho\pi}{2M}}\,x$
0	0
.1	.232
.2	.346
.3	.440
.4	.538
.5	.644
.6	.762
.7	.907
.8	1.110
.9	1.47
.95	1.864
1.0	∞

The apparent draft z can be related to the actual draft z', with respect to the undisturbed water surface by

$$z' = \pi/2\, f(\beta)\, z\,. \qquad (3.16)$$

which corrects the theoretical constant-force bottom contour empirically for pile-up. The function $f(\beta)$ can be determined from tests on the V-wedges.

In Chapter V this procedure is carried out for the $\beta_e = 20^\circ$ hull.

Chapter IV

EXPERIMENTAL EQUIPMENT AND PROCEDURE

The experimental equipment consists of (1) the drop mechanism, (2) the drop tank, (3) the accelerometer, (4) the model hulls, and (5) the cameras used to photograph the impact and the acceleration-time history. The testing is divided into (1) the procedure used in obtaining the impact pictures and (2) the procedure used in obtaining the acceleration histories.

Drop Mechanism

The drop mechanism consisted of a support and guide for a square metal rod. The rod was fabricated from hollow 3/4 in. x 3/4 in. square brass tubing. The model was attached to the rod by a 6 in. x 6 in. x 1/4 in. clear Lucite plate. The guide for the square rod contained eight ball bearings which restricted free movement to a vertical direction only.

Drop Tank

The model hulls were dropped into a rectangular wooden tank. A glass panel was set into the front of the tank. An adjustable metal plate was fastened to the inside of the back wall of the tank. This permitted the adjustment of the end gap between the sides of the tank and the ends of the model. The gap was kept at a minimum at all times to ensure two-dimensional flow.

A scale was attached at the edges and bottom of the glass panel to facilitate taking measurements from the photographs. The tank was set independent from the dropping mechanism. Four leveling screws were attached at the bottom outside corners of the tank to permit careful adjustment of the drop height. Wave absorbers and splash guides were attached to the ends of the tank. The absorbers and splash guides consisted of cellulose sponge cut to the required shape. These eliminated most of the splash resulting from the

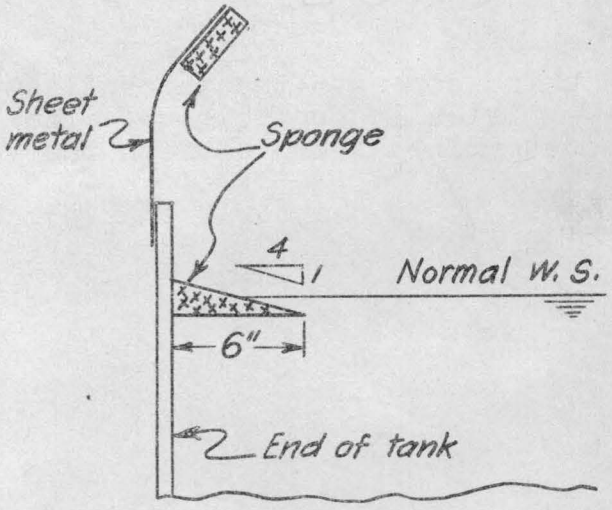

Fig. 4.1 Sketch of wave absorbers and splash guides

impact and quickly damped out surface disturbances after a test run. A hook gauge was fitted to one end of the tank to aid in careful adjustment of the water surface. Fig. 4.2 is a photograph showing the drop tank and support as used in this investigation.

Photography

The measurements of water pile-up were made from enlargements of 16 mm motion picture film by Bisplinghoff and Doherty. At best this was certainly difficult. Because of the importance of these measurements, a larger negative was specified for the investigation reported here. A 4- x 5-in. Speed Graphic camera with an f-2.8 coated Ektar lens was used for obtaining the photographs of the water pile-up. The aperture was set at f-5.6 and Ansco Super Pan Press film was used. The lighting was provided by an Ahbrams Portatron high-speed electronic flash gun. The pictures were all made at night or in a darkened room with the shutter set at 1 sec. so that the photography was essentially by "open-flash" technique.

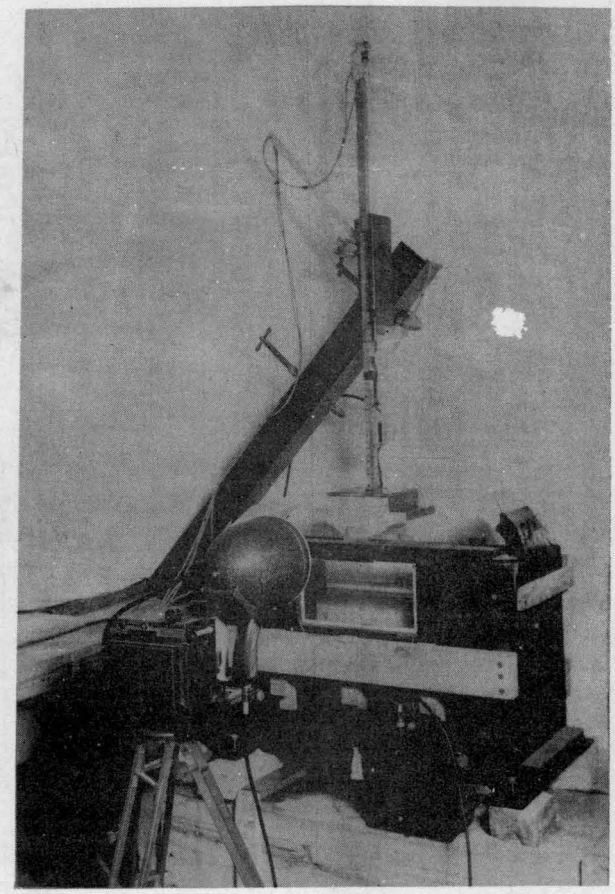

Fig. 4.2 Photograph of drop mechanism and equipment

The flash gun was "triggered" by a specially constructed acceleration switch mounted at the top of the model support rod (see Fig. 4.2). The switch contacts were actuated by a cantilever leaf of spring steel. By adjusting the spacing of the contacts, the time of the photographing relative to the initial impact, could easily be adjusted. A series of photographs showing the progressive growth of the water pile-up was thus obtained.

The negatives were enlarged to 8- x 10-in. photographs. From these photographs c, c', z, and z' were carefully measured. Typical photographs of the impact of the $\beta = 10°$, 20°, 30°, 40°, and 50° hulls are shown in Figs. 4.3, 4.4, 4.5, 4.6, and 4.7.

Accelerometer

The acceleration-time history was obtained using a Model 18C6 Calidyne accelerometer. The accelerometer was bolted to the hull cover plate. The shielded flexible accelerometer lead passed through the hull cover plate and was formed in a loop to permit unrestrained movement of the hull. This was similar to the arrangement used by Bisplinghoff and Doherty. This accelerometer employs a 5734 RCA mechano-electronic transducer. The accelerometer has a natural frequency of 250 cps. The signal from the accelerometer was passed through an oscilloscope and was then recorded from the oscilloscope screen by photography. Fig. 4.8 shows the circuit diagram of the accelerometer.

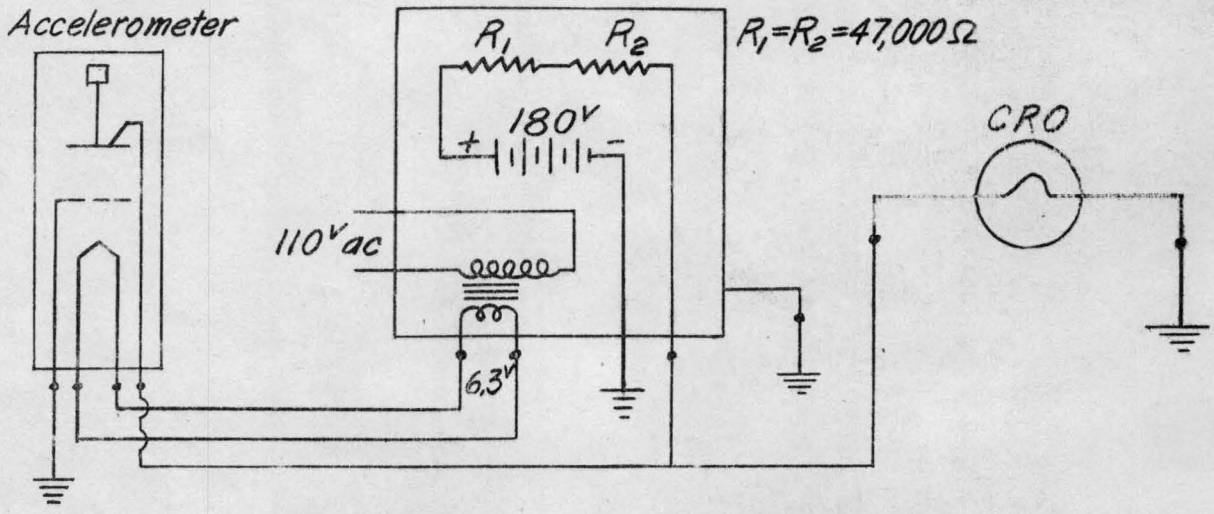

Fig. 4.8 Circuit diagram for Calidyne accelerometer

Fig. 4.3 Photograph of V-wedge during impact for $\beta = 10°$

Fig. 4.4 Photograph of V-wedge during impact for $\beta = 20°$

Fig. 4.5 Photograph of V-wedge during impact for $\beta = 30^{\circ}$

Fig. 4.6 Photograph of V-wedge during impact for $\beta = 40°$

Fig. 4.7 Photograph of V-wedge during impact for $\beta = 50^{\circ}$

Later the results were checked with a Statham Model A8-10-335 accelerometer. This was done because the Statham instrument was damped to about 0.7 of critical damping whereas the Calidyne accelerometer was only damped to 0.29 of critical. The recorded oscillograph records from the Calidyne instrument indicated that there may have been considerable "overshoot" at the instant of impact. Comparison of similar runs indicated that the Calidyne accelerometer did overshoot about 100 percent at the instant of impact. Therefore, only the results obtained with the Statham accelerometer are shown in this report.

Accelerometer-time Histories

The signal from the accelerometer was recorded from an oscilloscope screen by photographing with a Fairchild oscilloscope camera. The camera was equipped with an f-2.8 Wollensak coated lens mounted in a Rapax shutter and is equipped with a Polaroid-Land back. A print of the record can be obtained in a few minutes after exposure.

The oscilloscope was a Model 304A Dumont which was equipped with a special short-persistence blue cathode-ray tube and a driven sweep. This oscilloscope was specially designed for photographing these relatively low-frequency transient signals. Fig. 4.9 shows the oscilloscope and the Fairchild camera.

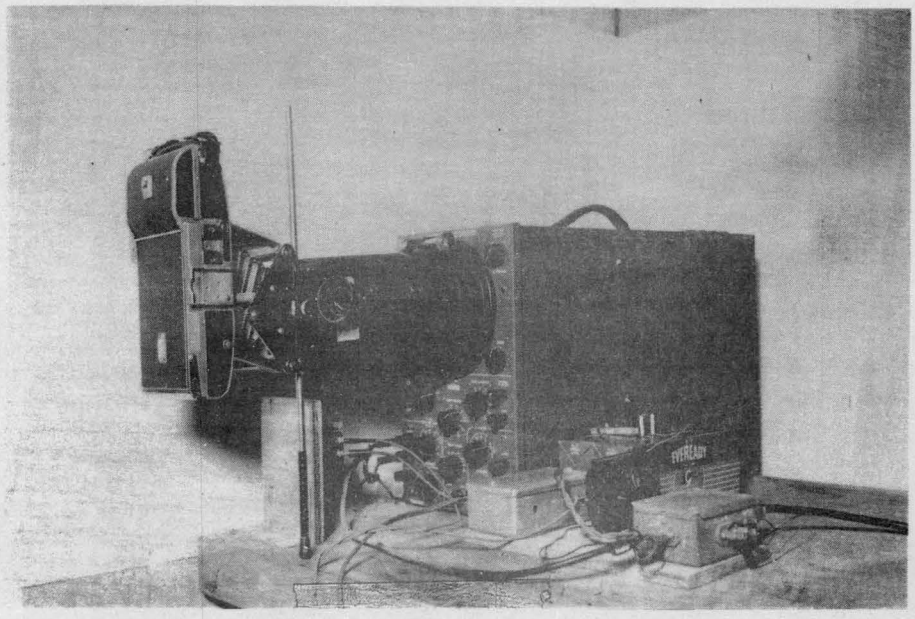

Fig. 4.9 Photograph of oscilloscope and camera

The shutter of the camera was set at "B" and operated by a solenoid. The solenoid was triggered by a roller micro-switch which was actuated by an adjustable plastic wedge attached to the side of the model support rod. The wedge was adjusted so that the shutter was opened at the point where the keel touched the water and remained open until the chines were immersed.

Model Hulls

All hulls were smoothly sanded and finished with 6 or 7 coats of Periseal. This resulted in a very smooth durable finish. The models were constructed of well seasoned solid mahogany.

The surface contours of all model hulls were cut using a horizontal milling machine. A pair of metal templates were cut from 16-gage sheet metal and carefully filed to proper shape. These templates then served as a guide for a guide wheel or follower at the end of the cutter head of the mill. If accurate templates are made, close tolerances of the hull can easily be attained. Fig. 4.10 shows a photograph of the milling operation on a 20° hull. The inside of the hull was hollowed out using an end mill in a vertical milling machine. Lead ballast was added as necessary to adjust the final weight of the hull. Fig. 4.11 shows the V-wedge hulls as they were used during the tests.

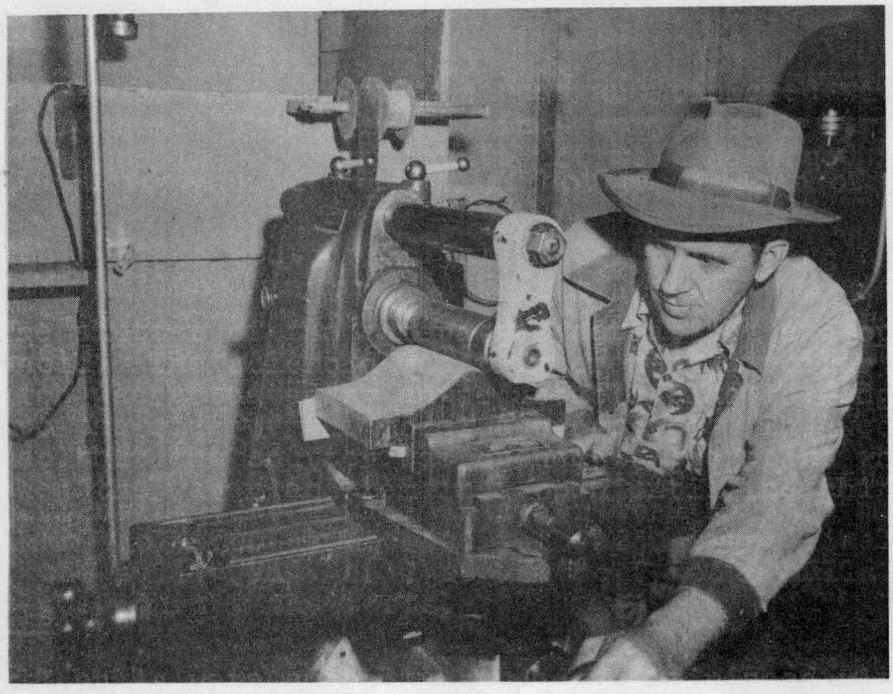

Fig. 4.10 Photograph of milling of bottom contour of model hull

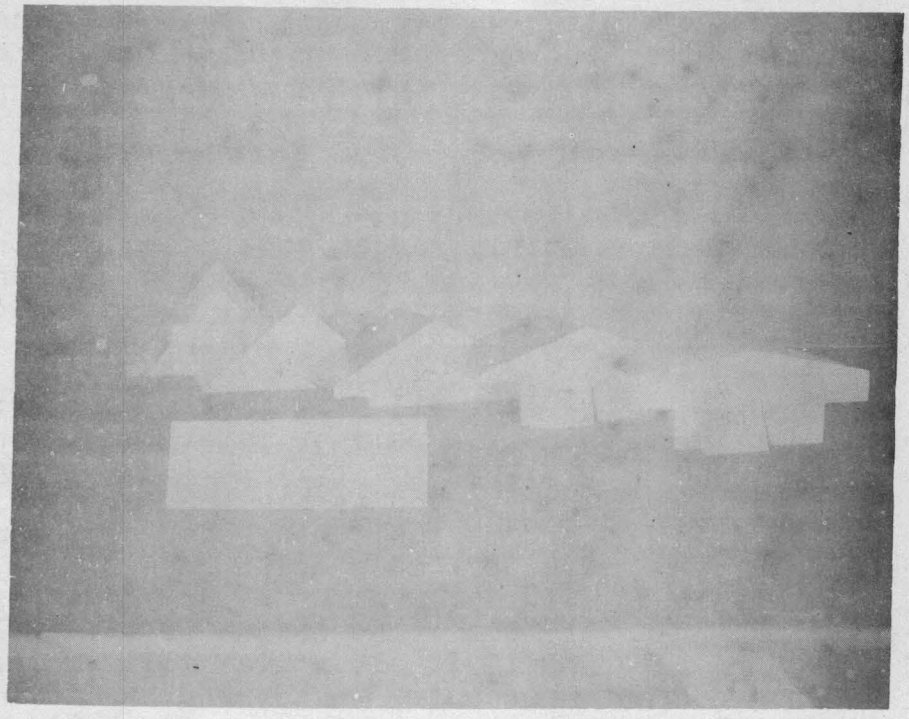

Fig. 4.11 Photograph of V-wedge hulls

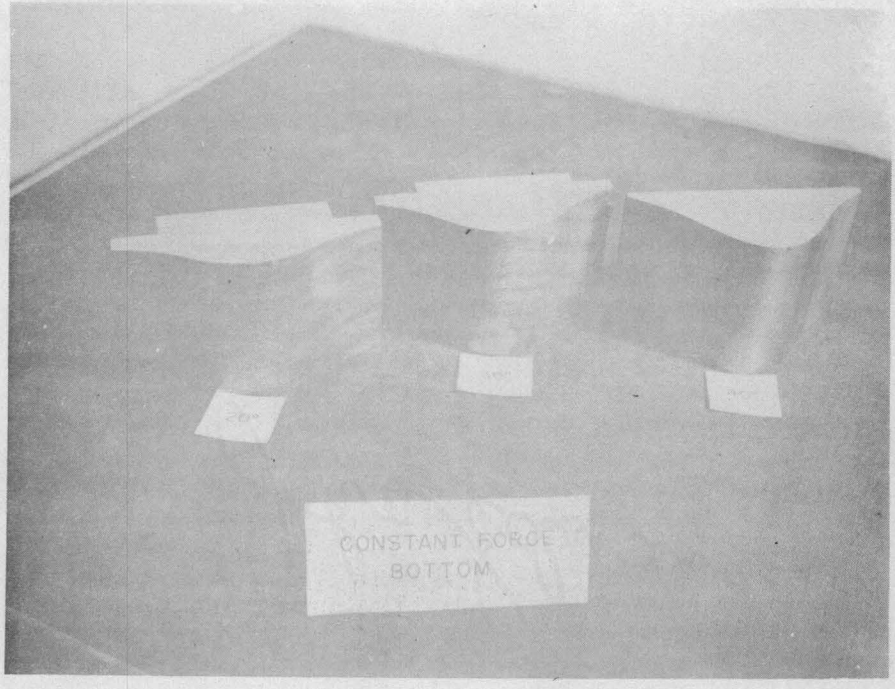

Fig. 4.12 Photograph of constant-force model hulls

Fig. 4.12 shows the three constant-force hulls corresponding to equivalent angles of deadrise of 20°, 30°, and 40°.

Testing Procedure

The hull to be tested was fitted to the hull cover plate using brass wood screws. A well-greased cork gasket was used between the hull and the plate. After tightening, the joint was sprayed with clear Krylon plastic spray. The support was raised to the proper height and the hull release set. The tank was then carefully leveled, the distance between the keel and the normal water surface adjusted to 5 in., and the water level adjusted to normal by adding or removing water. When the water surface was calm the test proceeded.

After each test the hull was raised and wiped to remove excess water. The acceleration switch for the flash gun was adjusted and the water surface again adjusted to replace any loss by splashing. The test proceeded as soon as the water became calm again.

The normal drop height was 5 in.; however, the hull of $\beta_e = 20°$ was also dropped from 3 in., 4 in., 6 in.; and 7 in. This yielded information on the effects of variation of the contact velocity.

The normal weight of the accelerating components of the apparatus was 4.32 lb(0.1345 slugs). The beam loading of the model was changed by the addition of lead ballast to the hull. The optimum hull of $\beta_e = 20°$ was also tested at a model beam loading of 5.38 lb(0.167 slugs), 6.45 lb (0.201 slugs), and 7.55 lb (0.235 slugs).

Chapter V

DISCUSSION OF RESULTS

The investigation was divided into three parts. The tests on the V-wedge hulls comprised the first part. The second part of the work included the testing and development of the constant-force bottom contour. The third part included the variation of the contact velocity and the beam loading.

Tests of the V-wedges

At least three good photographs of the water pile-up of each angle of deadrise were examined to obtain measurements of z, z', c, and c'. From these measurements, the dimensionless parameters $\frac{z-z'}{2c}$, z/z', and c/c' were computed. All of the values of the parameters obtained are tabulated in Table 5.1.

Table 5.1

Results of Tests on V-wedge Hulls

Run No.	Wedge	z/z'	$\frac{z-z'}{2c}$	c/c'	$f(\beta)$
4.1	10°	1.14	0.015	1.25	.0559
4.2	10°	1.19	0.0145	1.23	.0535
7.1a	10°	1.20	0.0155	1.19	.0531
7.2a	10°	1.16	0.0125	1.17	.0549
7.1	20°	1.23	0.035	1.21	.0518
7.2	20°	1.28	0.038	1.27	.0498
7.3	20°	1.21	0.0307	1.25	.0526
7.4	20°	1.23	0.0342	1.25	.0518
3.2	30°	1.36	0.081	1.23	.0468
3.3	30°	1.22	0.053	1.27	.0522
8.2	30°	1.30	0.063	1.34	.0490
8.3	30°	1.25	0.0566	1.263	.0510
8.4	30°	1.31	0.068	1.28	.0486
8.5	30°	1.29	0.065	1.32	.0494
8.6	30°	1.27	0.0605	1.29	.0502
6.1	40°	1.32	0.0995	1.33	.0483
6.2	40°	1.31	0.101	1.30	.0486
6.3	40°	1.31	0.100	1.32	.0486
6.4	40°	1.33	0.102	1.34	.0479
6.5	40°	1.41	0.121	1.39	.0452
5.2	50°	1.32	0.133	1.29	.0483
5.4	50°	1.32	0.146	1.34	.0483
5.6	50°	1.37	0.157	1.38	.0465

Fig. 5.1 shows a graph of c/c' plotted as a function of angle of deadrise, β. Eq. 2.5 is shown on this graph as well as the experimental points obtained by Bisplinghoff and Doherty (MIT data). The experimental points indicate no support for the theoretically derived Eq. 2.5. The MIT data indicate slightly higher values of c/c'; however, the trends between MIT data and the Colorado A & M data are parallel.

The greatest difference between the experimental points and Eq. 2.5 occurs at $\beta = 10^{\circ}$. This fact may explain why the theoretically-derived constant-force hull failed to develop the expected values of deceleration during the early part of the time history.

The ratio of the height of the pile-up compared to the wetted width $\frac{z-z'}{2c}$ is shown on Fig. 5.2 as a function of the angle of deadrise. The data indicate the least scatter at $\beta = 10^{\circ}$ and the most scatter at $\beta = 50^{\circ}$. This may be explained by the fact that relatively little pile-up occurs at $\beta = 10^{\circ}$ whereas the most pile-up occurs at $\beta = 50^{\circ}$. Furthermore, the pile-up at $\beta = 50^{\circ}$ may also be affected to a greater extent by surface tension or relative roughness of the hull. An average curve has been drawn through the data on Fig. 5.2.

The experimental values of function $f(\beta)$ have been plotted as a function of angle of deadrise on Fig. 5.3. A curve was fitted through these points. Typical water surface profiles for the different wedges are shown in Fig. 5.4.

No theory or explanation is offered for the large divergency between the theoretical equation and the experimental points. It is possible that the experimental techniques could be improved. Weible (6) pointed out that the use of high speed photographs of the immersion process of spheres and cylinders was not entirely satisfactory.

Tests of the Constant-force Hull

A comparison of the theoretical acceleration history with the actual acceleration history of the constant-force hull reported in reference 16 is shown in Fig. 5.5. The tests on the theoretically derived constant-force hull for $\beta = 20^{\circ}$ indicated that the acceleration did not peak as fast as was expected. The slope of the constant-force hull at the keel is zero because in this way the acceleration history would rise to the peak value immediately upon contact with the water. The angle of deadrise then gradually changes through small angles to a maximum of about 30° at approximately one-third the distance between the keel and the chine.

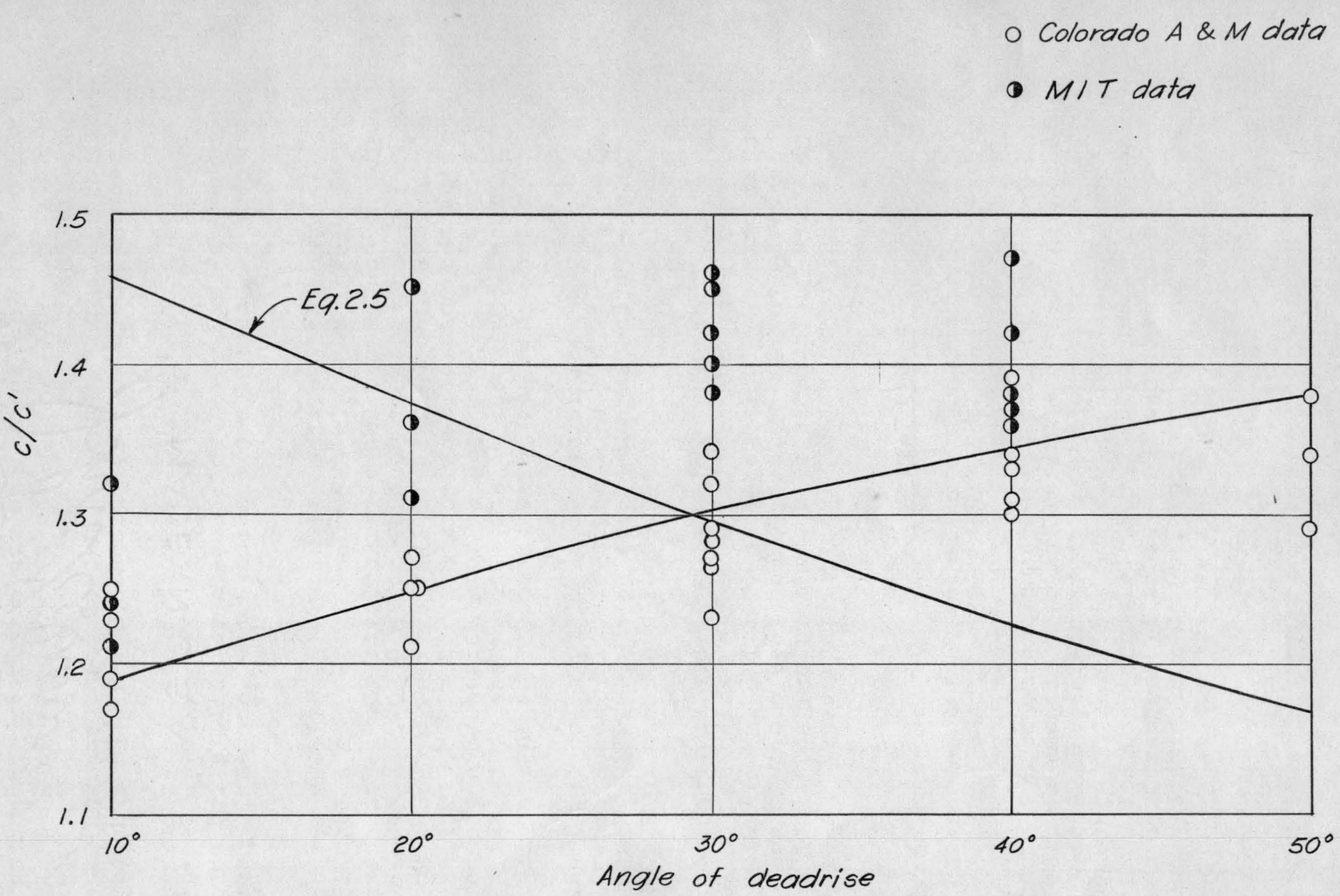

Fig. 5.1 Variation of water pile-up with angle of deadrise

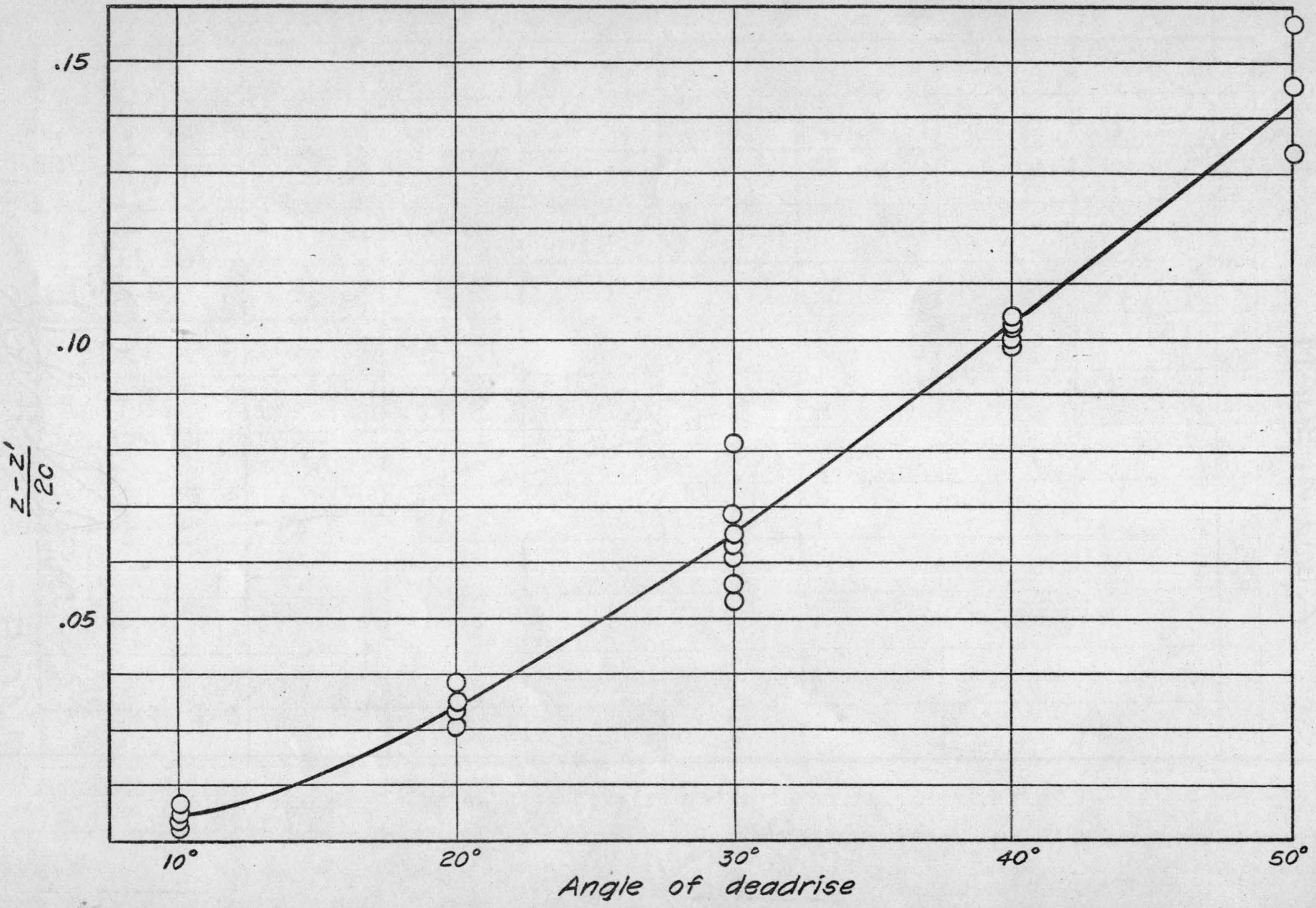

Fig. 5.2 Variation of width of water pile-up with angle of deadrise

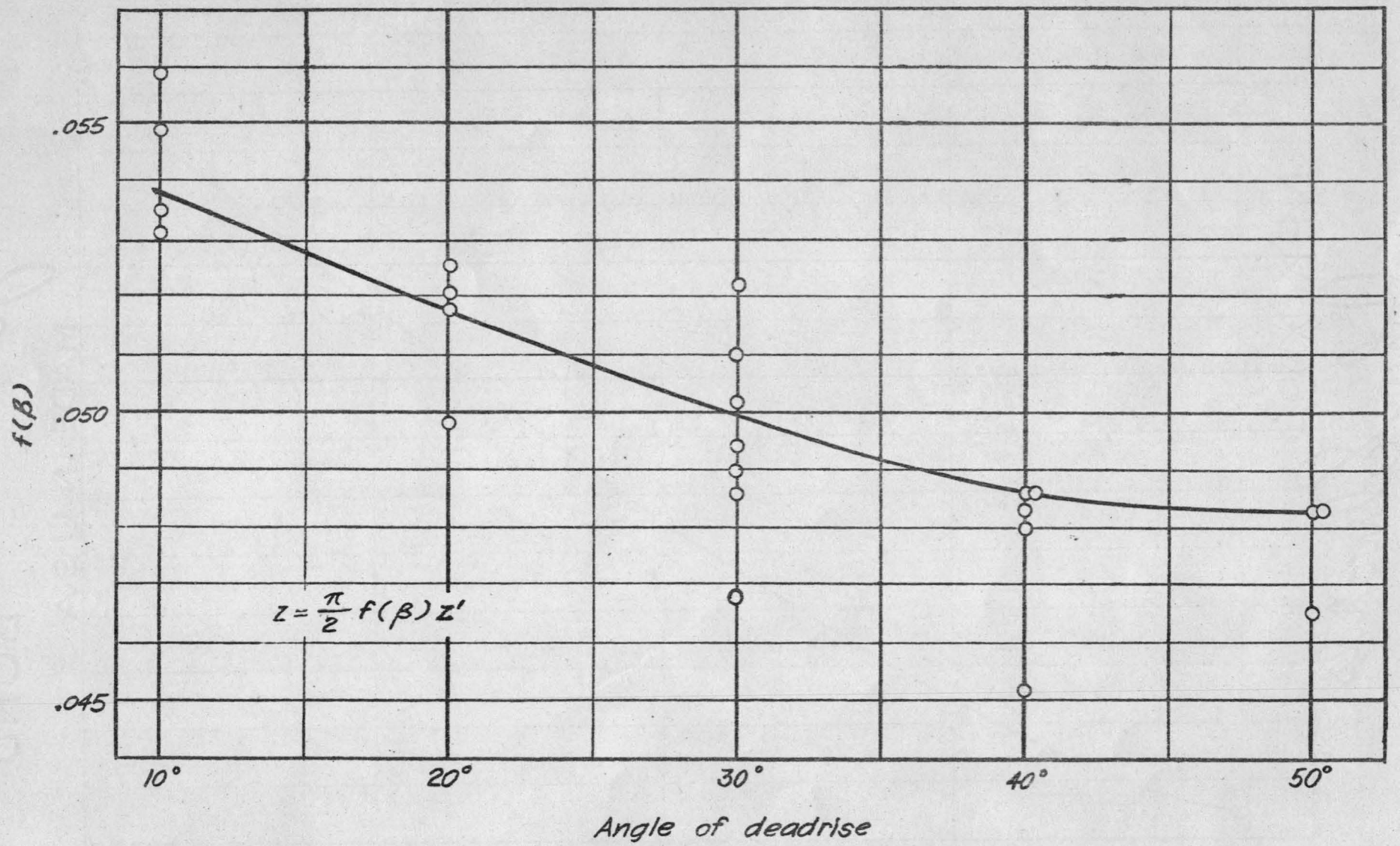

Fig. 5.3 Variation of f(β) with angle of deadrise

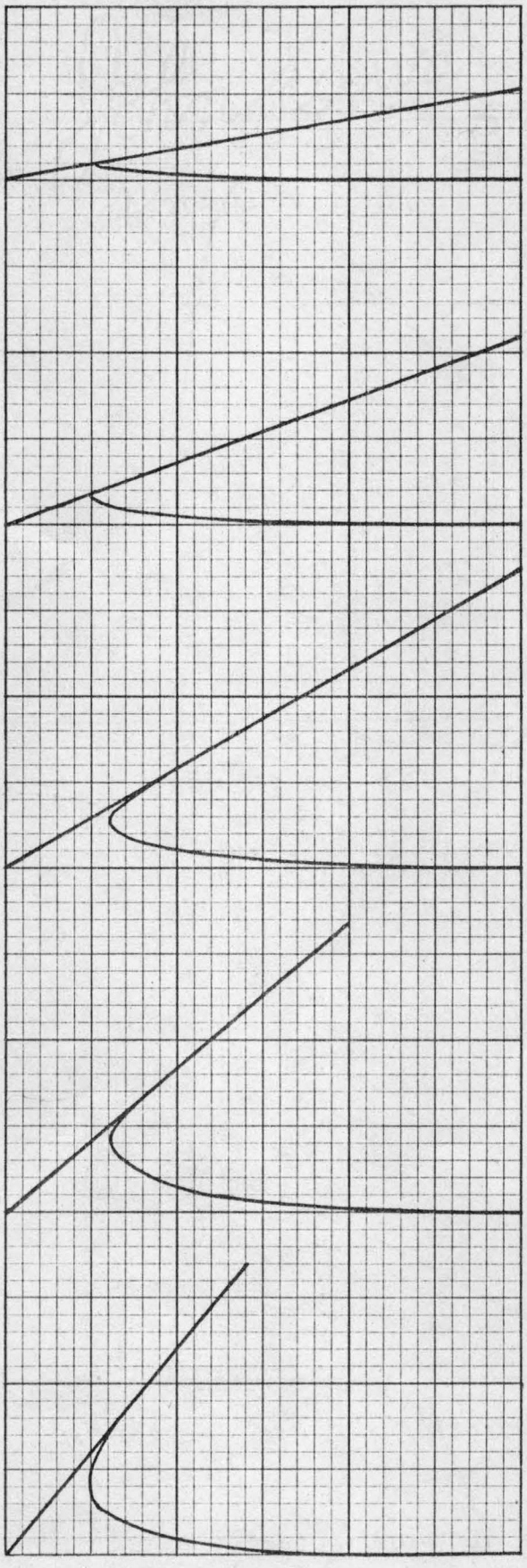

Fig. 5.4 Water surface profile for different V-wedges during impact

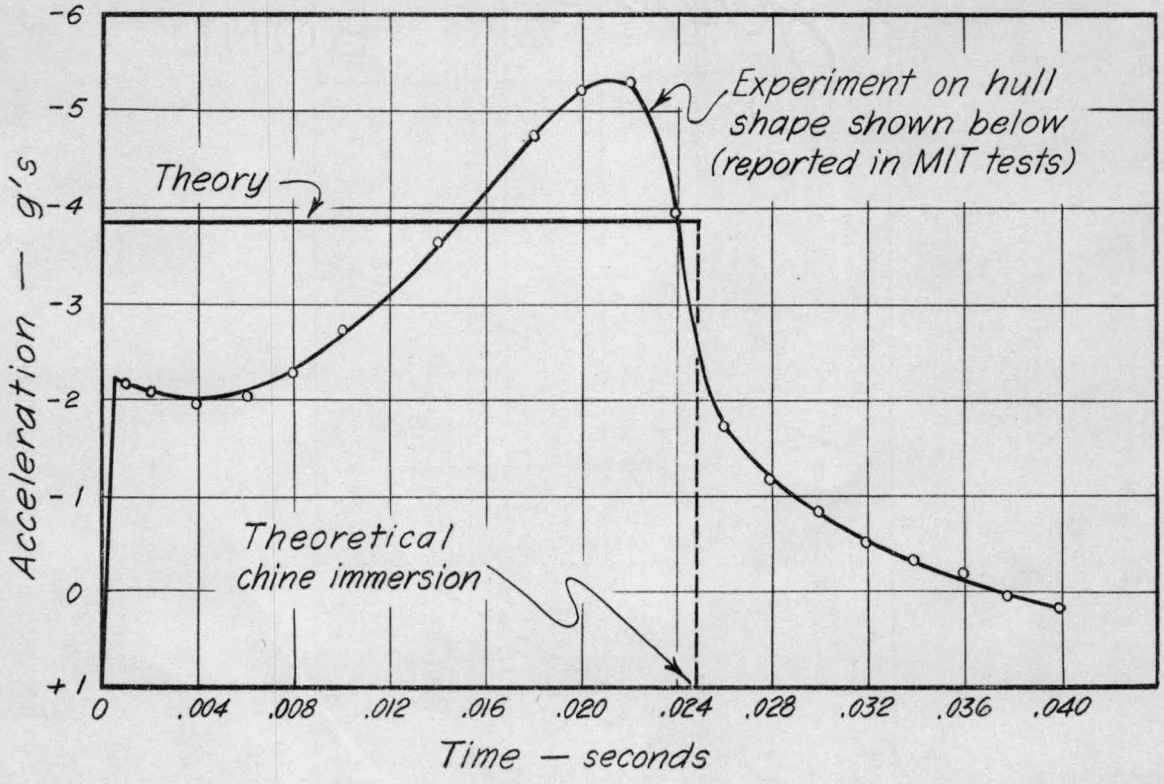

Fig. 5.5 Comparison of actual and theoretical performance of constant-force hull

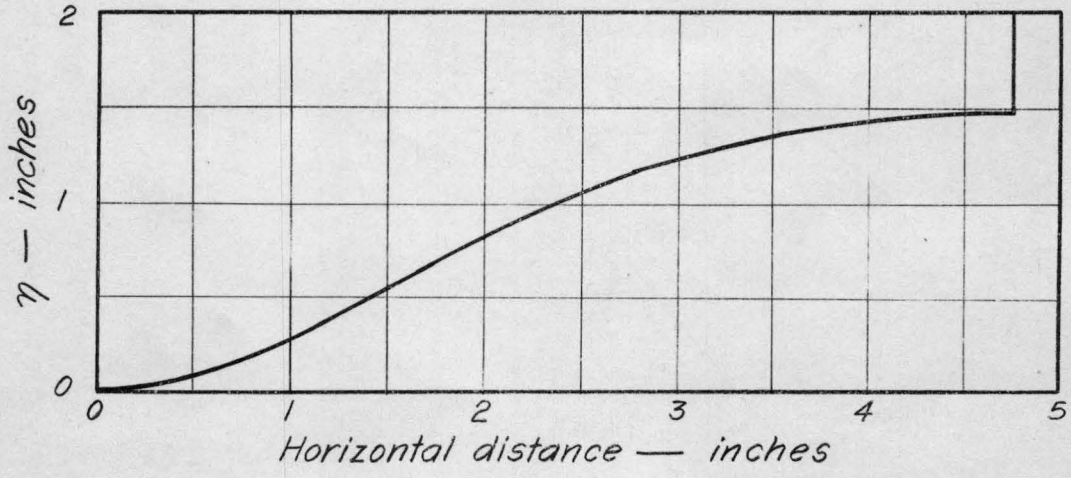

Fig. 5.6 Profile of the theoretical constant-force hull

Fig. 5.7 Photograph of theoretical constant-force hull during impact for $\beta_e = 20°$

Fig. 5.8 Photograph of constant-force hull during impact for $\beta_e = 20°$

Fig. 5.9 Photograph of constant-force hull during impact for $\beta_e = 40^\circ$

From the tests on the 10° V-wedge, it is known that the experimental value of acceleration does not attain the magnitude expected from the theory. If it can be supposed that the angles of deadrise less that 10° behaved in a similar manner, then it could be deduced that the constant-force hull needed to be flatter over a greater portion of its keel area. Only in this way would the acceleration-time history rise to the maximum quickly. In a similar manner it can be assumed that the hull should have a slightly steeper angle of deadrise near the chines; thus the peak in the latter part of acceleration history can be avoided.

The coordinates of the theoretically derived hull were used as a beginning point. The steps for correcting the coordinates are outlined below.

1. Successive coordinates, z_1 , z_2 , z_3 .... z_c , were chosen along the contour.

2. The angle of deadrise, β_1 , β_2, ... β_c , was measured to each point.

3. For each value of angle of deadrise, the $f(\beta)$ term was determined from Fig. 5.3.

4. The corrected value for each coordinate, z'_1 , z'_2 .... z'_c was computed from the equation
$z' = \pi/2 \, f(\beta) \, z$.

5. The revised contour is the curve drawn through values of z'_1 , z'_2 .... z'_c .

The first hull produced by this procedure did not yield the uniform acceleration history. After a number of hulls were corrected by this procedure, the final optimum contour was intuitively derived by simultaneous examination of the previous hull contours and their acceleration-time histories.

Constant-force Hull Contours for Various Angles of Deadrise

The hull finally developed by the preceding procedure had an equivalent angle of deadrise of 20°. The angle between a horizontal line at the keel and through the chine was 20°. Hulls of equivalent 30° and 40° were produced from the dimensionless plot of the 20° hull. The actual hull contours and their acceleration-time histories are shown on Figs. 5.10 and 5.11 and the dimensionless form of the constant-force hull contour is shown on Fig. 5.12.

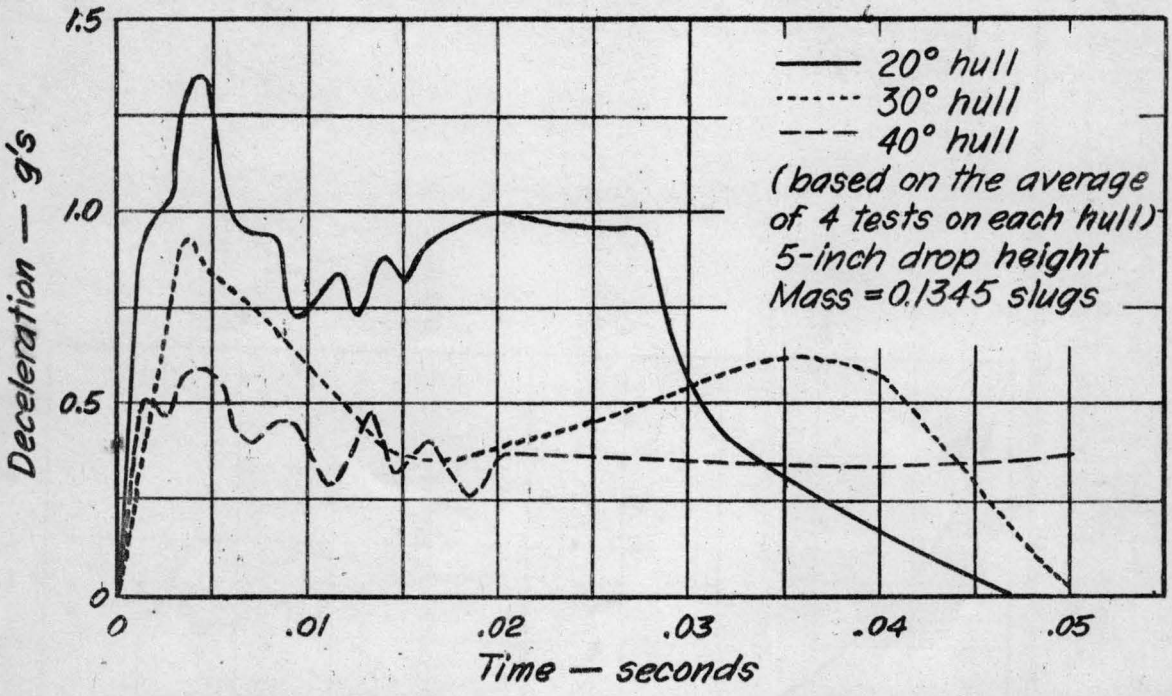

Fig. 5.10 Acceleration-time histories for constant-force hulls

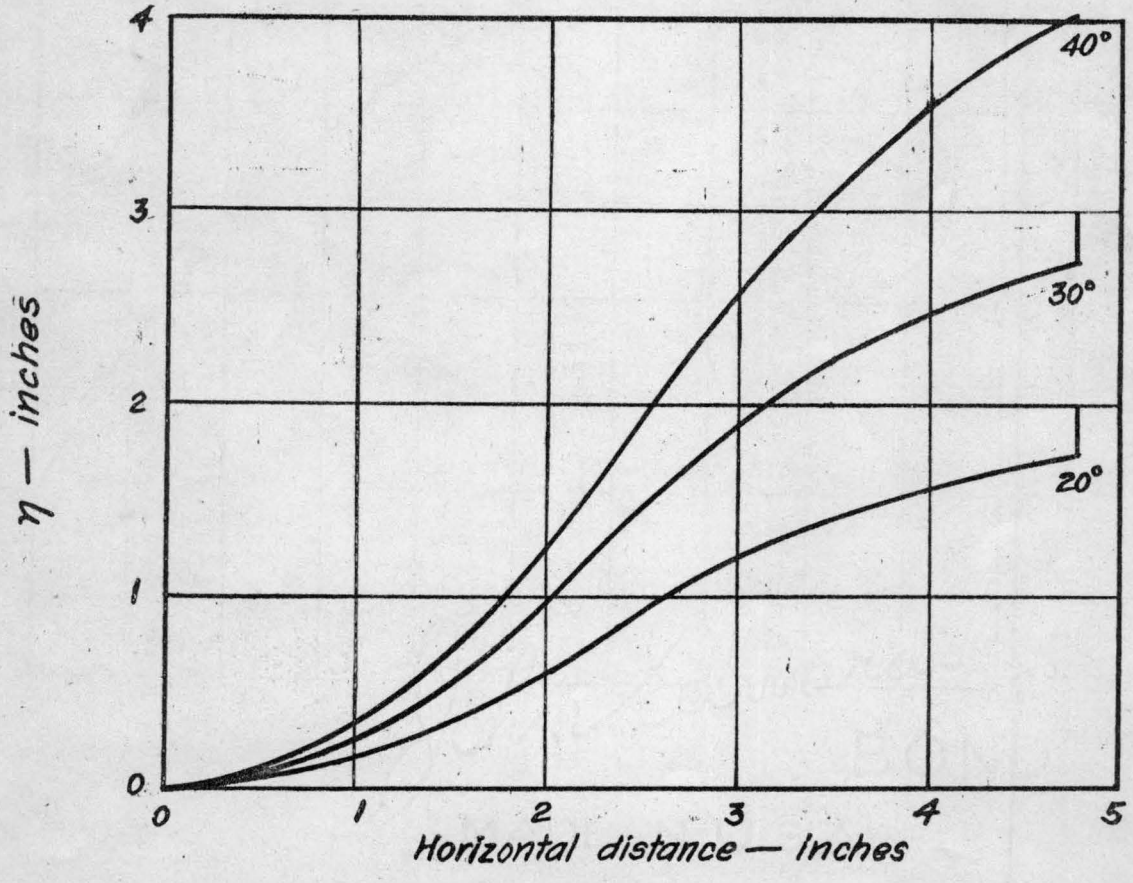

Fig. 5.11 Profile of constant-force hulls

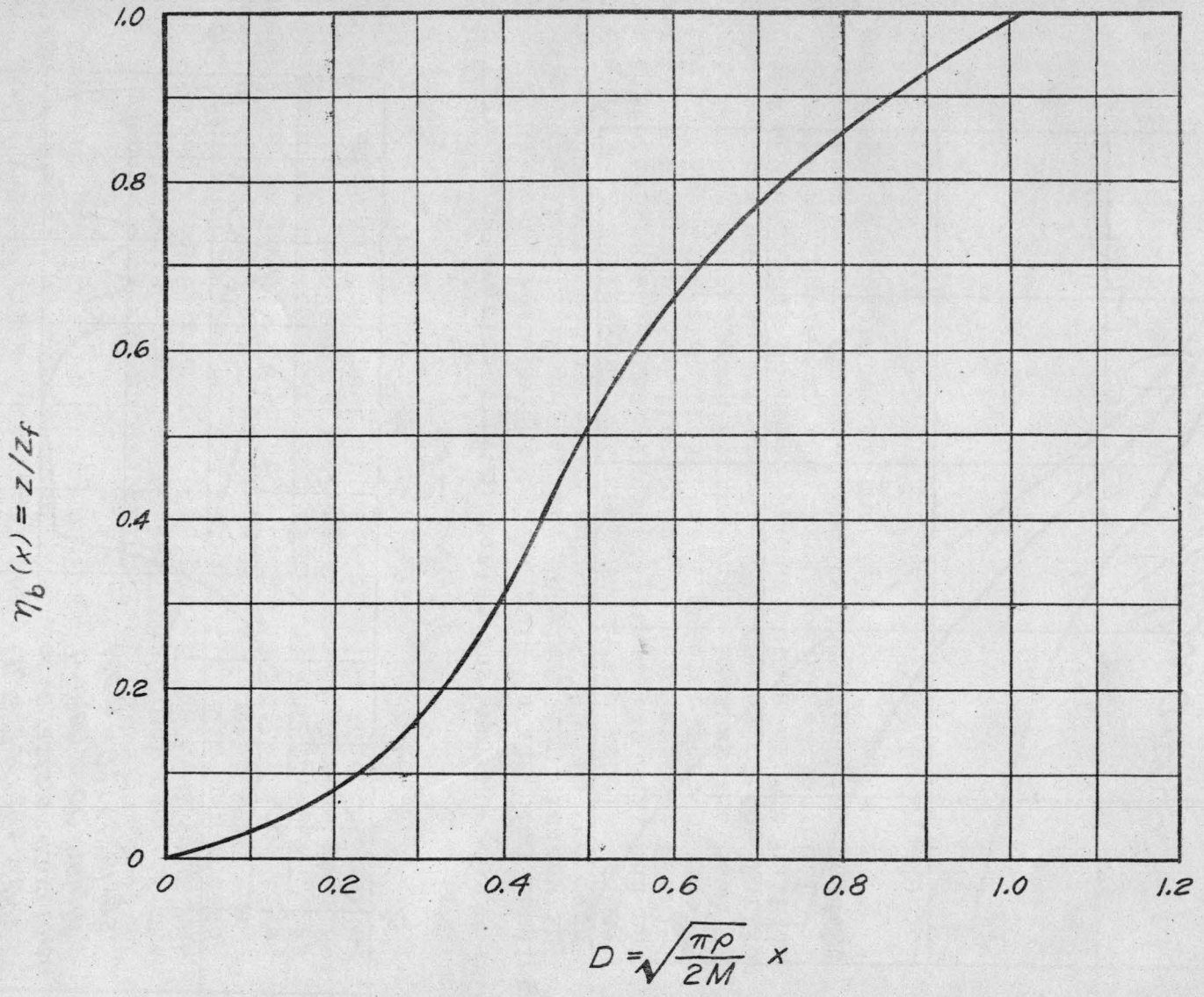

Fig. 5.12 Dimensionless coordinates of constant-force hull

Variation of Contact Velocity

The contact velocity was varied by changing the drop height. Drop heights used were 3 in., 4 in., 5 in., 6 in., and 7 in. The constant-force hull for $\beta_e = 20^\circ$ was used for these tests. A comparison of the acceleration histories for these drop heights is shown on Fig. 5.13.

These acceleration histories seem to be composed of two parts as distinguished by two peaks. The first peak of the acceleration history occurs on contact of the keel with the water. The second peak of the acceleration history occurs when the flat area near the chines makes contact with the water. The balance of these two peaks is rather sensitive as is shown by the acceleration histories on Fig. 5.13. As the velocity of contact is increased, the keel area develops a greater part of the force of deceleration than the chine area.

Variation of the Beam Loading

The test gross weight of the hull is the beam loading for the two-dimensional case. The deceleration history in terms of the hull mass is shown on Fig. 5.14. As the mass of the hull is increased, the area under the acceleration-time curve decreases. This indicates that the hull had not come to rest by the time the chines were immersed. Examination of Fig. 5.14 also indicates a greater part of the kinetic energy is absorbed by the chine area as the beam loading of the hull is increased. The energy of the falling hull was not entirely absorbed by the bottom of the hull but was absorbed by increasing the displacement of the hull after the chines were immersed and is therefore independent of the shape of the bottom of the hull.

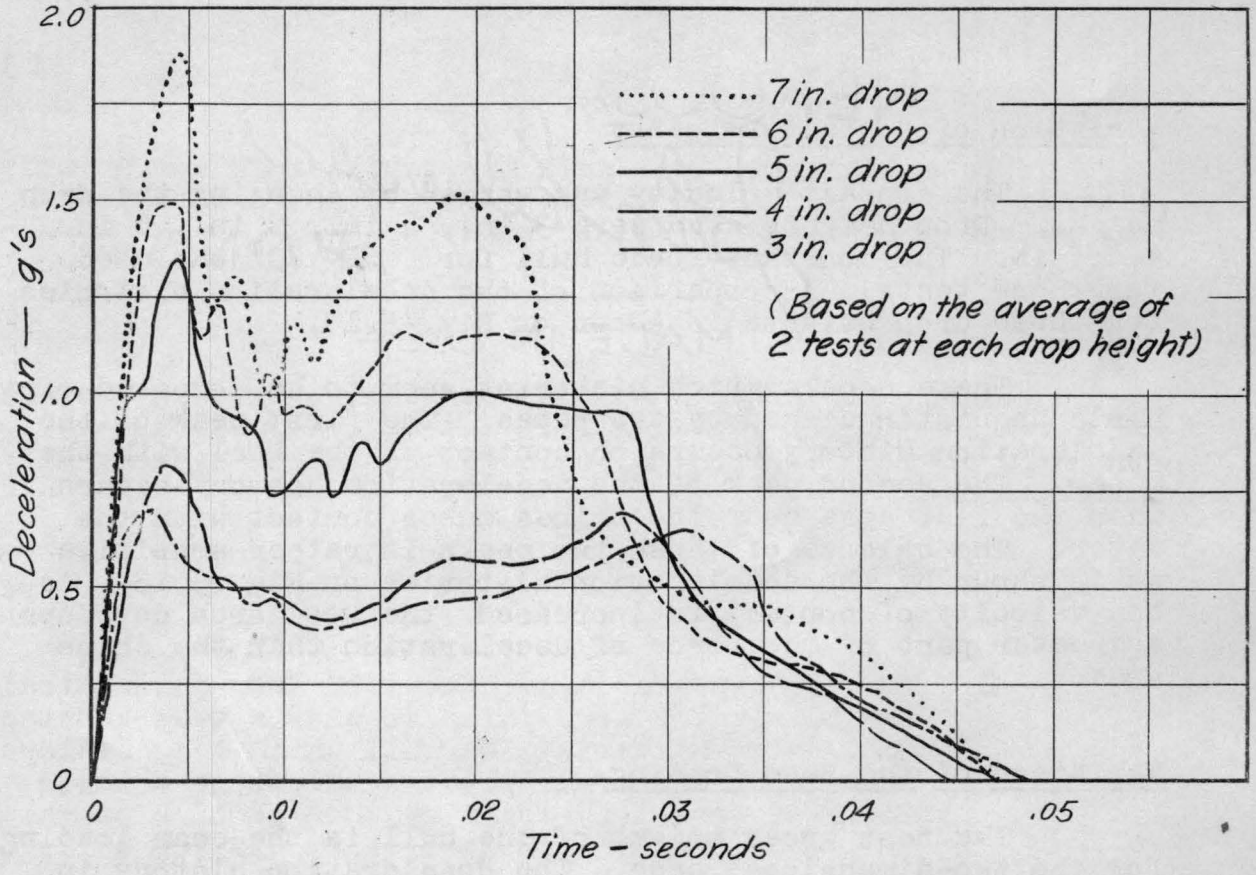

Fig. 5.13 Effect of contact velocity on acceleration history for constant-force hull when $\beta_e = 20^\circ$

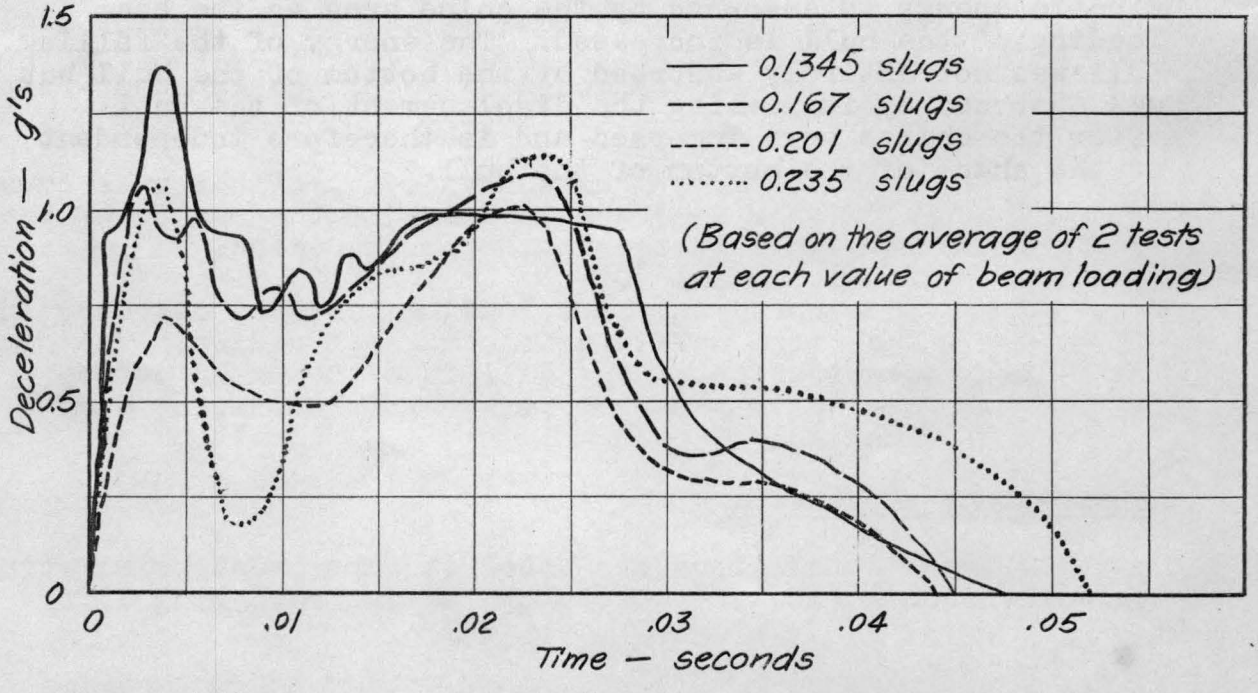

Fig. 5.14 Effect of beam loading on acceleration history for constant-force hull when $\beta_e = 20^\circ$

Chapter VI

SUMMARY

In summarizing this work the conclusions are briefly listed, together with the limitations of the results and the recommendations for further study.

Conclusions

These experiments suggest certain changes in the shape of a seaplane hull, especially in the region just forward the main step. The results indicate the following general conclusions:

1. The theory fails to predict the water pile-up for the V-wedges. This is particularly true for small angles of deadrise.

2. The constant-force hull derived from theoretical considerations also fails to give a true constant-force time history. The hull which was developed by a trial and error process maintains a lower angle of deadrise over a greater portion of the keel area than the theoretically derived hull.

3. The tests on the constant-force hull indicates that the peak deceleration can be reduced from 4.5 g's for the 20° V-bottom to 3.3 g's for the 20° constant-force bottom.

4. Constant-force bottoms having an equivalent angle of deadrise of 30° and 40° can be built from the non-dimensional coordinates of the constant-force bottom.

5. Increasing the contact velocity of the hull causes a greater increase in force in the region of the keel than in the region of the chine.

6. Increasing the beam loading caused a decrease in the force developed on the keel region. The penetration of the hull into the water before coming to rest increased with increasing beam loading.

Limitations of Results

These conclusions are based on experiments simulating two-dimensional flow and a seaplane having zero wing lift.

The practical case of a seaplane landing is complex. The factors of forward speed, sinking speed, and the presence or absence of waves interpose great differences between actual operational conditions and the conditions of these experiments.

Recommendations for Further Research

Additional information about the impact of V-wedges of angles of deadrise of 10° or less would be useful. The use of ordinary photographs only to measure the pile-up phenomenon for the flat hulls is not entirely satisfactory, and possibly a more satisfactory method could be developed.

REFERENCES

1. von Kármán, Th.: 'The Impact of Seaplane Floats During Landing'. N.A.C.A. T.N. No. 321, 1929.

2. Kreps, R. L.: 'Experimental Investigation of Impact in Landing on Water'. N.A.C.A. T.N. No. 1046, 1943.

3. Monaghan, M. A.: 'Theoretical Examination of Effect of Deadrise in Seaplane-Water Impacts'. Royal Aircraft Establishment Technical Note No. Aero. 1989, 1949.

4. Milwitzky, Benjamin: 'A Generalized Theoretical and Experimental Investigation of the Motions and Hydrodynamic Loads Experienced by V-Bottom Seaplanes During Step-Landing Impacts'. N.A.C.A. T.N. 1516, February, 1948.

5. Bisplinghoff, R. L. and Doherty, C. S.: 'A Two-dimensional Study of the Impact of Wedges on a Water Surface'. MIT, March, 1950.

6. Weible, A.: 'The Penetration of Bodies with Various Head Forms at Perpendicular Impact on Water'. Forschungsanstalt Graf Zeppelin, Stuttgart, Germany. NRL Translation No. 286.